Polymer gel combustion synthesis of LiFePO$_4$/C composite as cathode material for Li-ion battery

Rajeev Sehrawat · Anjan Sil

Abstract LiFePO$_4$/C has been synthesized by polymer gel combustion method. Of aniline monomer, 0.5 and 1.0 ml were used for the different amount of gel formation. The particle sizes of LiFePO$_4$/C composites designated as lithium iron phosphate (0.5) (LFP(0.5)) and LFP(1.0) were estimated as ~400 and ~100 nm for the powders synthesized with 0.5 and 1.0 ml of monomers, respectively. The final particle size of the LiFePO$_4$/C depends on the initial monomer content used in the synthesis process. Thicknesses of carbon coating on the particles of LFP(0.5) and LFP(1.0) powders, as revealed by TEM observation, are ~3 and ~7 nm, respectively. The sample LFP(1.0) delivers discharge capacities of 72 and 60 mAh g^{-1} which are higher than those of LFP(0.5) at fast discharging rates of 5 and 10 C. The higher rate capability of sample LFP(1.0) was due to small particle size, low charge transfer resistance, and higher Li$^+$ diffusion coefficient as compared to LFP(0.5).

Keywords LiFePO$_4$ · Coating · Raman spectroscopy · Electrochemical properties · Polyaniline

Introduction

Olivine-structured lithium iron phosphate (LFP) has attracted a great interest as a cathode material for the Li-ion battery since the study on this material was reported by Padhi et al. [1]. The LFP has several advantages as compared to the other commercially available cathode materials. But the main drawback of this material is the low conductivity and slow Li$^+$ diffusion [2]. These shortcomings restrict this material from its commercial applications in the field of lithium ion battery. In order to overcome these drawbacks, several attempts viz. (1) doping the material with foreign atoms, (2) surface coating of the powder, and (3) particle size reduction, have been made [3–5]. The doping increases the conductivity of material but the presence of foreign atom in the crystal lattice of LiFePO$_4$ may be deleterious if it occupies on the Li$^+$ sites [6]. Particles size reduction improves the kinetics of intercalation/de-intercalation processes. Lowering the particle size reduces the diffusion length resulting in reduction of the diffusion time according to the relation, $T=L^2/2D$, where L is diffusion length and D is diffusion coefficient. All these factors enhance the discharge capacity of the material at a faster current rate [6]. However, particles having a size smaller than a certain limit in nano-size range show poor cycling performance because of difficult processability to mix conducting carbon black with LFP active material for cathode fabrication [7]. The conductive surface coating (such as with carbon and conducting polymer) has been widely used to increase the electronic conductivity [8–10]. Although carbon coating improves the rate capability of LiFePO$_4$, it effects adversely on the tape density. So, the amount of carbon must be optimized to achieve the higher rate capability and higher tap density [11]. As the Li$^+$ intercalation/de-intercalation takes place only along [010] direction, continuous/complete coating is required to produce LFP-based cathode materials for high C-rates [12]. A rate of 1 C is defined as the rate at which a cathode of capacity X mAh, while discharging under ideal condition should deliver a current of X mA for 1 h. However, a continuous or complete surface coating is difficult to grow [13]. The continuous/complete carbon coating was achieved by in situ polymerization restriction method [14] in which the authors have demonstrated to grow polyaniline to cover the primary crystallites of FePO$_4$, and the polyaniline further decomposes to yield residual carbon on the surface of LFP.

R. Sehrawat (✉) · A. Sil
Department of Metallurgical and Materials Engineering, Indian Institute of Technology Roorkee, Rookee 247667, India
e-mail: rajeev.sehrawat@gmail.com

In the present work, the carbon-coated LFP was prepared by in situ polymerization of polyaniline on sol-gel-synthesized LiFePO$_4$ and completely decomposing the polyaniline to convert into carbon coating. The present process differs from the earlier reported work [14] that no additional carbon sources such as sucrose or glucose were added to assist the process of complete polymer decomposition into carbon for continuous carbon coating. The process adopted in the present work has yielded relatively well graphitized and uniform carbon coating.

Experimental

Synthesis

The synthesis of LiFePO$_4$/C (LFP/C) was performed in two steps. In the first step, two solutions were prepared separately with 0.5 and 1.0 ml of aniline monomer (99.5 %, GR, Merck) containing 2.62 g of (NH$_4$)H$_2$(PO$_4$) (99 %, GR, Merck) in 200 ml of millipore water. The mixing was carried out on a magnetic stirrer for 30 min, and during the process, 3.7 g of FeCl$_3$ (98 %, Merck) dissolved in 100 ml of millipore water was added dropwise into the solutions. FePO$_4$ precipitates (white) starts forming instantaneously in the solution. The solution, initially white in color, turns into light green due to the formation of polyaniline on the surface of FePO$_4$ particles 4 h after the addition of aqueous solution of FeCl$_3$. The solution was further heated for 2 h at 65 °C to increase the growth of polyaniline and color of the solution changes from light green to dark green. The solution was heated between 95 and 100 °C under continuous stirring to evaporate the water content, and after 6–8 h of heating, a dark green residue of solid polymer gel was formed on the surface of NH$_4$Fe(HPO$_4$)$_2$. The formation of NH$_4$Fe(HPO$_4$)$_2$ particles takes place during the evaporation of water content. In the second step, the synthesized material was ground in a pestle-mortar with Li(CH$_3$COO) (99 %, Loba Chemie) maintaining a molar ratio of 1:1 between Li and Fe. The mixture was heated at 400 °C for 4 h under the Ar(90 %) + H$_2$(10 %) gas flow and was further grinded in a pestle-mortar for 30 min to homogenize. The material was heated at 700 °C for 15 h under Ar(90 %) + H$_2$(10 %) atmosphere. The calcined material was further washed thoroughly with deionized water and acetone to remove chloride impurity to get pure LFP/C powder.

Characterization

The morphology of polymer gel and LFP was observed by using field emission scanning electron microscope (FESEM) (FEI, Quanta 200F). The energy dispersive X-ray analysis (EDAX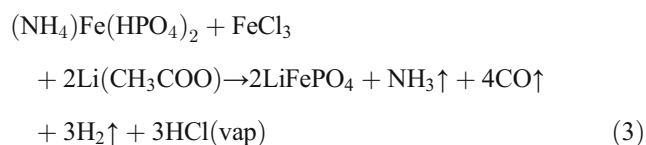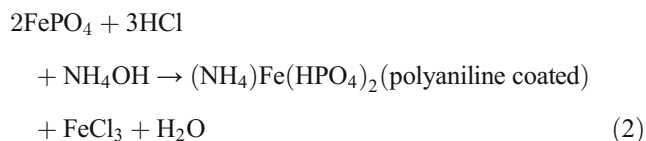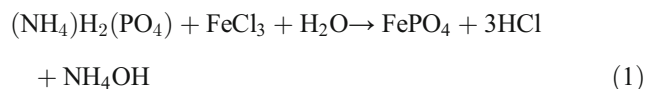) was performed to obtain the elemental composition of the samples. The polymer gel of polyaniline was characterized using Fourier transform infrared spectroscopy (FTIR) analysis (UV-1500, Shimadzu Japan). The carbon coating on the LFP particles was confirmed by transmission electron microscopic (FEI-TECHNAI-20) observation at an operating voltage of 200 kV. Raman confocal micro-spectrometer system (inVia, Renishaw) was used to characterize the carbon for its graphitization. He-Ne LASER with a 514-nm wavelength as the excitation source was used to obtain Raman spectra of the material. The X-ray diffraction pattern of polymer gels and LFP were obtained on X-ray diffractometer (Bruker AXS, D8 advance) using CuK$_\alpha$ radiations (λ = 1.5418 Å) with a scanning rate of 1.5° min^{-1} and the phase analysis of the pattern was performed using X-ray diffraction software (PANalytical, X'Pert HighScore Plus 2.2.0). The weight fraction of the carbon in the LFP/C composites was determined by thermogravimetric analysis of the samples using thermal analyzer (Seiko Instruments, EXSTAR TG/DTA 6300).

Cathode fabrication and testing

Cathodes were prepared with LFP active material (70 wt%), PVDF binder (15 wt%), and carbon black (15 wt%). Initially, the active material and carbon black were dry mixed and then slurry was made by adding binder and NMP. The slurry was spread uniformly on aluminum foil using doctor blade technique. The material on foil was dried at 80 °C for 48 h under a vacuum and was further pressed using a hydraulic press for 30 min at a pressure of 500 kN m^{-2} to develop good adherence of the cathode material with the foil. The foil coated with the material was punched in a circular disk having an area of 1 cm^2 containing the 1–3 mg cm^{-2} of the material. Teflon cell was assembled for the electrochemical testing of the cathodes prepared with a lithium foil as counter electrode separated by polypropylene microporous separator membrane. The movement of Li$^+$ was through the electrolyte solution of LiPF$_6$ (1 M) in a solution of ethylene carbonate and dimethyl carbonate (EC/DMC = 1:1). The cell was assembled in an argon gas-filled glove box with a controlled atmosphere. The electrochemical impedance spectroscopy was performed on electrochemical testing system (Gamry Instruments) in the frequency range of 100 kHz–0.1 Hz by applying AC oscillations of amplitude 5 mV. The galvanostatic charging/discharging and cyclic voltammetry tests were performed in the respective voltage ranges of 2.2–4.2 V and 2.2–4.1 V on a battery testing system (BT2000, Arbin Instruments). Cell assembling and testing were performed in argon gas-filled glove box (MBRAUN, MB 200G) maintaining oxygen and moisture level of <0.1 ppm.

Results and discussion

The reaction during the synthesis of LFP/C is shown below:

$$(NH_4)H_2(PO_4) + FeCl_3 + H_2O \rightarrow FePO_4 + 3HCl$$
$$+ NH_4OH \tag{1}$$

$$2FePO_4 + 3HCl$$
$$+ NH_4OH \rightarrow (NH_4)Fe(HPO_4)_2 (\text{polyaniline coated})$$
$$+ FeCl_3 + H_2O \tag{2}$$

$$(NH_4)Fe(HPO_4)_2 + FeCl_3$$
$$+ 2Li(CH_3COO) \rightarrow 2LiFePO_4 + NH_3\uparrow + 4CO\uparrow$$
$$+ 3H_2\uparrow + 3HCl(\text{vap}) \tag{3}$$

The product of Reaction (2) is the polymer gel containing $(NH_4)Fe(HPO_4)_2$ and $FeCl_3$. The polyaniline-coated $(NH_4)Fe(HPO_4)_2$ was calcined with $Li(CH_3COO)$ at 700 °C. The calcined material was thoroughly washed with deionized water and acetone to remove the residual chlorine to get the pure LFP/C compound. The schematic diagram of complete synthesis process of LFP/C was shown in Fig. 1.

Structural analysis

The XRD pattern of polymer gel-coated $(NH_4)Fe(HPO_4)_2$ is shown in Fig. 2. The polymer gel formation was considered in two cases of 0.5 ml aniline and 1.0 ml of aniline additions. The samples synthesized with 0.5 ml aniline and 1.0 ml aniline are designated as aniline(0.5) and aniline(1.0). The diffraction peaks of the XRD pattern correspond to $(NH_4)Fe(HPO_4)_2$ matched with data base file JCPDS no. 01-085-1141 implying the formation of single-phase material. The broad and low intensity peak of the polyaniline which appears at ~25° is not observed in the XRD patterns (Fig. 2) [15]. This is perhaps due to negligible contribution of the polyaniline content to give rise to perceptible intensity in the pattern.

Figure 3 shows the XRD pattern of LiFePO₄/C composites designated as samples LFP(0.5) and LFP(1.0) synthesized using 0.5 and 1.0 ml of aniline monomers, respectively. The peaks in XRD pattern match well with the pattern of LiFePO₄ (JCPDS card 01-081-1173) having orthorhombic crystal structure with space group Pnma (62). The cell parameters were calculated using XRD data and the values are $a = 10.3154$ Å, $b = 5.9949$ Å, and $c = 4.6808$ Å giving a unit cell volume $V_{cell} = 289.4597$ Å^3 for sample aniline(0.5), and $a = 10.3212$ Å, $b = 6.0041$ Å, and $c = 4.6794$ Å giving a unit cell volume $V_{cell} = 289.9802$ Å^3 for aniline(1.0). No peak corresponding to carbon is present in the XRD patterns and this may be due to negligible amount of the carbon present in the sample to give rise to perceptible intensity in the pattern. Moreover, the carbon seems to be in disordered form, as was also evident by the Raman spectra of the materials.

Morphology studies

The FESEM micrographs of the solid polymer gel are shown in Fig. 4 which reveal the layered morphology of the polyaniline formed on the surface of $(NH_4)Fe(HPO_4)_2$ particles. The FESEM micrograph confirms that the average particle size of the sample aniline(1.0) is <100 nm and is smaller than sample aniline(0.5) having a particle size in the range of 200 to 400 nm. This is due to the fact that larger quantity (1.0 ml) of polyaniline have posed a size limit on the inorganic oxide particles grown. Agglomeration of $(NH_4)Fe(HPO_4)_2$ particles is also evident from the FESEM micrographs of both aniline(1.0) and aniline(0.5). If the amount of initially added aniline monomer is higher, then the amount of the polyaniline becomes high and particle size limitation takes place early.

Beyond an optimum amount (=1 ml) of monomers, the separate polyaniline rod formation takes place as confirmed by SEM microstructure Fig. 4c. With the aniline monomer limited to <0.5 ml, the formation of polyaniline is insufficient and partial coating develops as observed under SEM Fig. 4d. The polymer films subjected under SEM often leads to the development of film cracking at the operating voltage suitable for inorganic oxide material characterization. The cracking in the polymer coat as indicated by the arrow mark in one of the micrograph is an indirect evidence of the polymer films that was formed during the synthesis.

Figure 5 shows the FESEM micrograph of synthesized LFP/C. The micrograph confirms agglomeration of particles through the carbon present on the surface of LFP particles. EDAX confirms the presence of Fe, P, O, and C. As estimated by EDAX, the molar ratio of Fe, P, and O is near to 1:1:4. The FESEM micrograph shows that the crystallites of LFP synthesized using sample aniline(0.5) have a larger particle size (~500 nm) than that synthesized using aniline(1.0) (~100 nm) and this fact was further confirmed by TEM images. The particle size of $(NH_4)Fe(HPO_4)_2$ before calcination and of LFP after calcination was nearly the same, showing that final particle size of LFP remains unchanged during calcination process at 700 °C.

FTIR spectra of polymer gel-coated $(NH_4)Fe(HPO_4)_2$

FTIR spectra of aniline(0.5) and aniline(1.0) samples prepared with KBr are shown in Fig. 6, which confirm the formation of

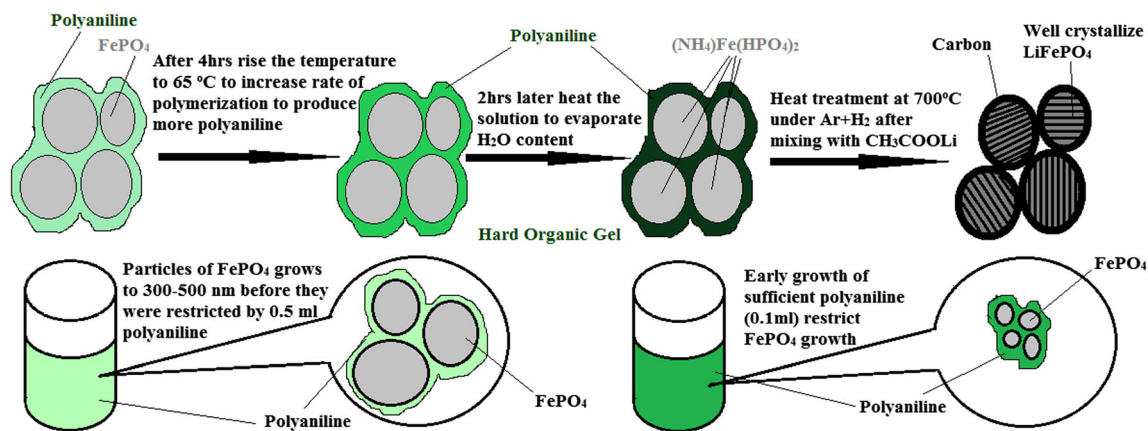**Fig. 1** Formation of polymer gel coating on $(NH_4)Fe(HPO_4)_2$ phase

polyaniline. The spectrum of the sample aniline(0.5) shows the peaks at 507, 614, 898, 1,055, 1,134, 1,240, 1,426, and 1,625 cm^{-1}, whereas 508, 614, 891, 1,053, 1,133, 1,244, 1,422, and 1,625 cm^{-1} are the peak positions for the sample aniline(1.0).

The bands at 507 and 508 cm^{-1} are due to bending deformation in polyaniline aromatic ring [16]. The 614 cm^{-1} peaks for aniline(0.5) and aniline(1.0) were assigned to C–H out of plane bending vibration in benzene ring of polyaniline [17]. Vibration corresponding to C–H out of plane bending in 1,2,4-tri-substituted ring gives rise to the peaks at 898 and 891 cm^{-1}, and the peaks occur when synthesis is done in ammonium-rich solvent [16]. The peaks at 1,055 and 1,053 cm^{-1} are attributed to internal mode of vibration of PO_4^{-3} ions [18]. The characteristic shoulder peak of polyaniline at 1,134 and 1,133 cm^{-1} due to Q=N=Q (Q is quinoid benzene ring of polyaniline) stretching was observed and appears to be very weak due to PO_4^{-3} group [19]. The peaks at 1,240 and 1,244 cm^{-1} are due to C–N stretching in polyaniline (BBB) ring [16]. The broad peaks at 1,426 and 1,422 cm^{-1} are one of the three deformations due to ν_4 mode. The absorption band at 1,625 cm^{-1} is

attributed to the bending vibration of oxygen in water molecule [20].

Raman spectroscopy of LFP/C

The structure of carbon formed due to the decomposition of polymer is of great importance as the electrochemical properties of LFP are greatly affected by the structure of carbon. The structural formation of carbon on the surface of LFP was characterized by using Raman spectroscopy. The Raman spectra of LFP(0.5) and LFP(1.0) are shown in Fig. 7. The two broad bands at 1,350 and 1,590 cm^{-1} represent D-band and G-band of graphitic carbon vibration. The G-band originates due to the formation of highly ordered graphitic carbon and assigned to E_{2g} optical mode. The E_{2g} mode is doubly degenerate Raman active optical mode where carbon atoms move in graphene plane toward and away from each other [21, 22]. The D-band occurs due to breakage of symmetry viz. finite size of graphite with edges treated as defects and stacking disorder [23]. The different forms of carbon growth can be assessed by the shape of D-band. I_D and I_G are defined as

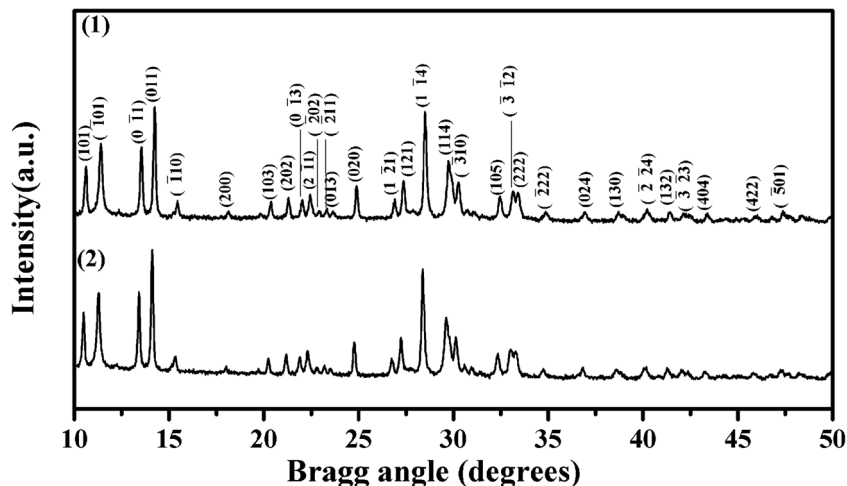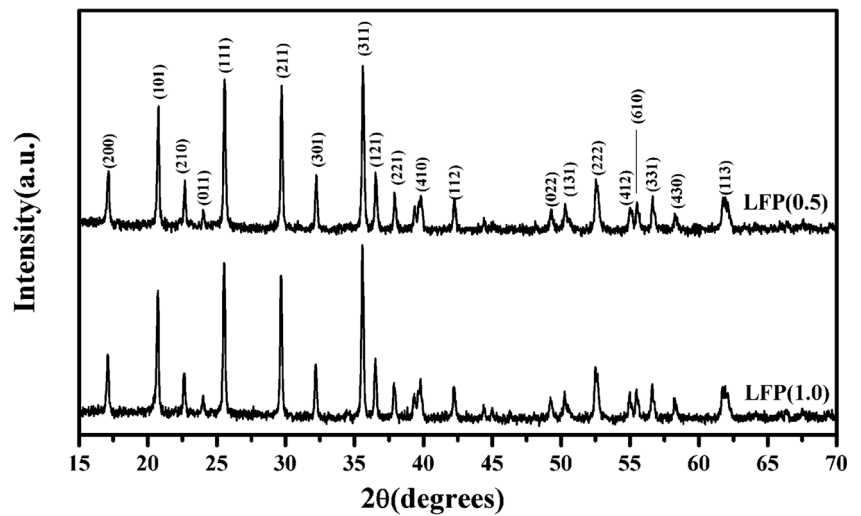**Fig. 2** XRD patterns of (*1*) aniline (0.5) and (*2*) aniline (1.0)

Fig. 3 XRD patterns of LFP(0.5) and LFP(1.0) showing all the peaks indexed

intensities of defect and graphitized bands, respectively; the intensity ratios ($R=I_D/I_G$) have been calculated from the pattern given in Fig. 7. The R values are 0.70 and 0.74 for carbon coatings generated with 0.5 and 1.0 ml aniline monomer used in the synthesis of LFP/C, showing that the amount of graphitized carbon is more than the carbon in disordered form [24]. The formation of graphitic carbon in the coating is essential as

it favors the electronic conductivity through the carbon network during charging/discharging of cell.

TEM analysis of LFP/C

The transmission electron microscopy was performed to observe the carbon distribution and particle morphology of

Fig. 4 The FESEM micrograph of **a** aniline(1.0), **b** aniline(0.5), showing the crack in thin polymer coating on the (NH4)Fe(HPO4)2, **c** polymer-coated $(NH_4)Fe(HPO_4)_2$ synthesized using 1.5 ml aniline showing individual polymer rods formation, and **d** polymer-coated $(NH_4)Fe(HPO_4)_2$ using 0.2 ml aniline showing partial coating
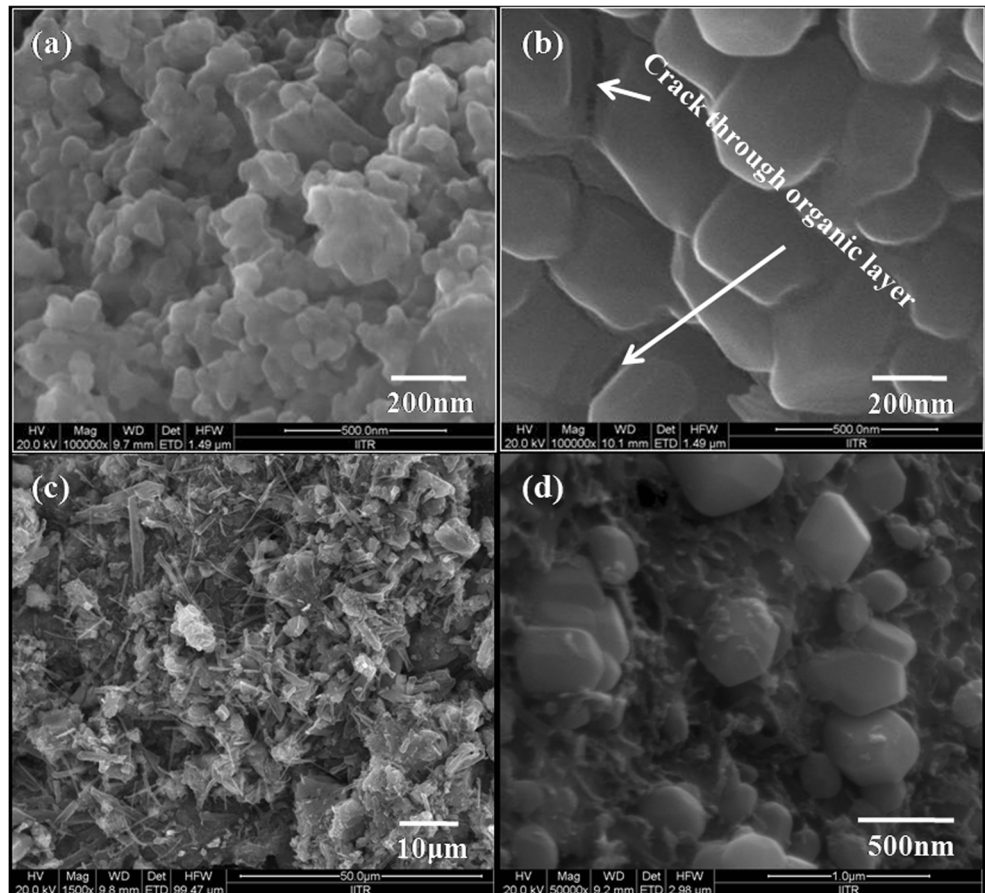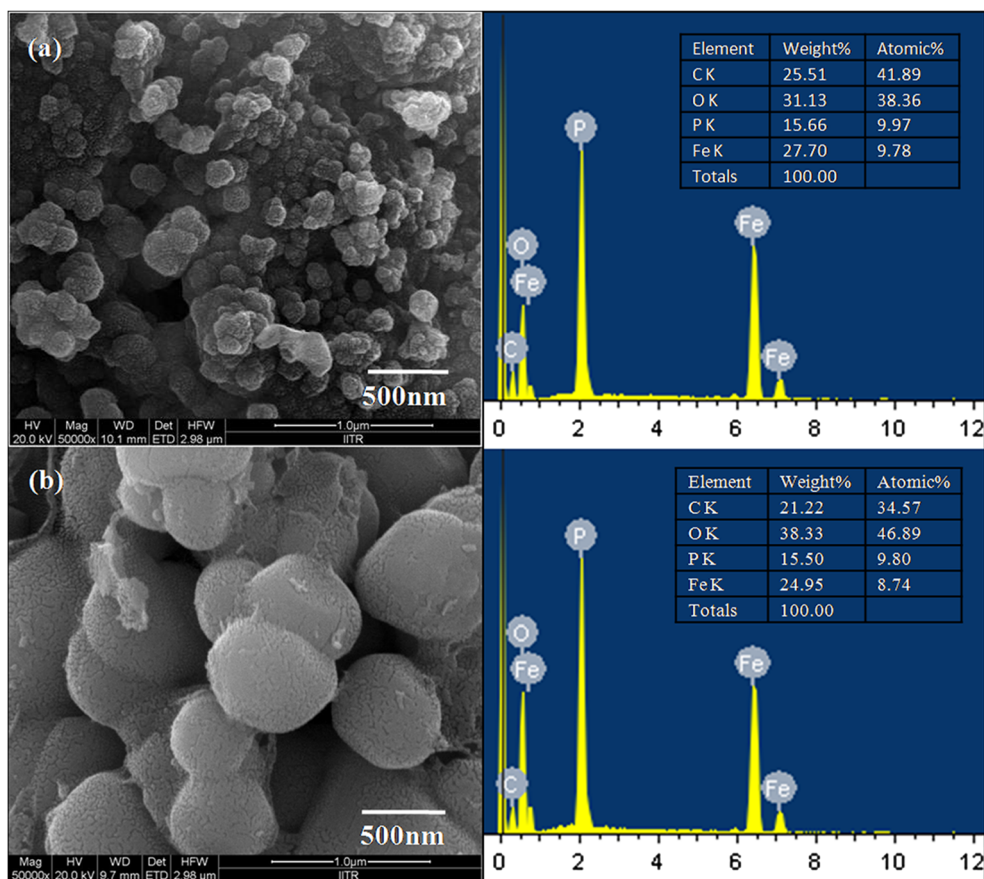
Fig. 5 **a** FESEM micrograph of LFP(1.0), particle size ~100 nm, and **b** FESEM micrograph of LFP(0.5), particle size ~500 nm, and EDAX spectra showing presence of C, O, P, and Fe

Element	Weight%	Atomic%
C K	25.51	41.89
O K	31.13	38.36
P K	15.66	9.97
Fe K	27.70	9.78
Totals	100.00	

Element	Weight%	Atomic%
C K	21.22	34.57
O K	38.33	46.89
P K	15.50	9.80
Fe K	24.95	8.74
Totals	100.00	

LFP(0.5) and LFP(1.0) samples. TEM images in Fig. 8a and c show the particles of LFP(1.0) and LFP(0.5) are nearly of spherical shape. The particles of LFP(1.0) are <100 nm and particles of LFP(0.5) lie in the size range of 300–500 nm. The TEM images in Fig. 8a and c show that LFP particles are joined with each other under the cover of continuous and complete carbon coating. However, the degree of particle agglomeration is more in the case of LFP(1.0) compared to LFP(0.5). The HRTEM images clearly show the amorphous carbon shells form a continuous coating on LFP particles having shell thicknesses of ~3 and ~7 nm for samples LFP(0.5) and LFP(1.0), respectively. Interconnectivity of the particles via carbon coating helps to enhance the electrical conductivity of bulk materials. The graphitized carbon shell is the path of electrons movement through the surface of particles during charge/discharge cycles of the electrode prepared with the synthesized materials LFP/C.

Thermogravimetric analysis LFP/C

Thermogravimetric (TG) analysis of samples LFP(1.0) and LFP(0.5) was performed in air atmosphere from room temperature to 750 °C. Oxidation of LFP starts at 300 °C and the reaction completes at 600 °C to produce two phases $Li_3Fe(PO_4)_3$ and Fe_2O_3 [25]. Due to the oxidation, weight gain by the material LFP was estimated to be 5.07 %. Further, in the temperature range between 350 and 500 °C, carbon combustion from the surface of LFP/C also takes place. Hence, the total carbon content in LFP/C material can be estimated by taking into account of the weight gain due to oxidation.

$$\text{Carbon content (wt\%)} = \text{Total wt. loss(wt\%)} + 5.07 \quad (4)$$

From the TG traces (Fig. 9) of samples LFP(1.0) and LFP(0.5), a minor weight loss of ~0.50 and 0.16 % was observed by heating the samples up to 150 °C due to moisture release. The net weight loss between 300 and 600 °C was estimated to 4.60 and 0.45 wt% for LFP(1.0) and LFP(0.5) samples and according to above equation; the estimated weight percent of carbon was 9.67 and 5.52 for the samples LFP(1.0) and LFP(0.5), respectively. Carbon combustion that occurs between 350 and 500 °C is also evident from the TG trace of the samples. The weight loss between 360 and 450 °C is quite significant for the sample LFP(1.0), whereas nominal in the case of LFP(0.5). The marginal weight gain by the samples beyond 450 °C shows the oxidation process
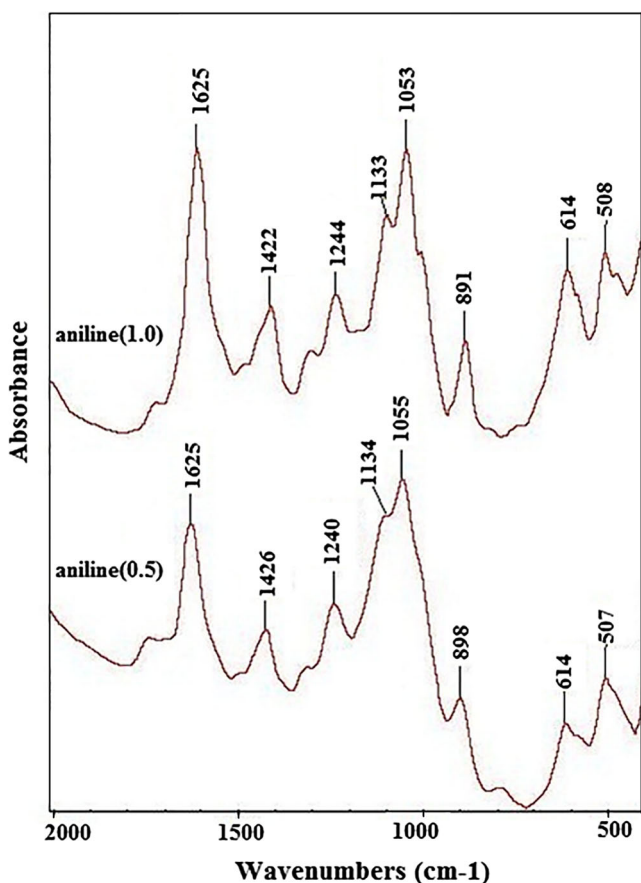
Fig. 6 FTIR spectra of aniline(1.0) and aniline(0.5)

decomposition of 0.8671 and 0.4386 g of polyaniline yields ~0.3686 and 0.2076 g of carbon as coating material on the surface of LFP.

Electrochemical impedance spectra

The electrochemical impedance spectra of samples LFP(1.0) and LFP(0.5) were performed to know the conducting behavior. Figure 10a shows that the impedance spectra are semicircle profile in high to middle frequency and inclined straight line on real impedance axis in a low-frequency region. The profiles of impedance spectra can be explained by equivalent circuit of the Nyquist plot shown in the inset of Fig. 10a. The high frequency intercept on real impedance axis corresponds to bulk resistance (R_b) of the electrochemical cell, offered by the separator, electrode, and electrolyte. Medium frequency intercept on real impedance axis corresponds to R_{ct} is attributed to charge transfer resistance on the interface of electrode and electrolyte [26]. The straight line starting from the edge of medium frequency side of semicircle to low-frequency region corresponds to Warburg impedance which reflects the Li$^+$ diffusion in the cathode electrode [27]. The sample LFP(1.0) and LFP(0.5) shows R_{ct} values of 500 and 710 Ω, respectively. Low charge transfer resistance deliver by sample LFP(1.0) is due to good electronic conductivity provided by carbon rich LFP(1.0) sample. Although the carbon layer is also present on the surface of LiFePO$_4$ particles for sample LFP(0.5), the particle of sample LFP(1.0) have a sufficient amount of carbon in the coating region to give better coverage. The better coverage of LiFePO$_4$ particles by carbon provides enhanced conductivity to the electrode.

The electrochemical reversibility of the electrode material can be determined by a current density factor which can be calculated by using the following relation [28]:

continues even after the completion of the complete carbon removal.

In a control experiment, 1.0 and 0.5 ml aniline monomers were made to undergo polymerization in the presence of FeCl$_3$ to find out the polymer yields which were found to be 0.8671 and 0.4386 g, respectively. The yields were estimated to be ~85 and ~86 % for 1.0 and 0.5 ml aniline, respectively. The experimental results are summarized in Table 1. So,

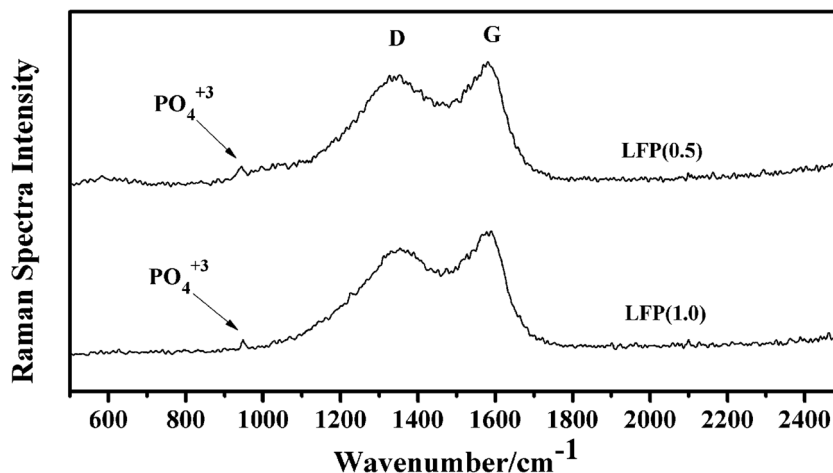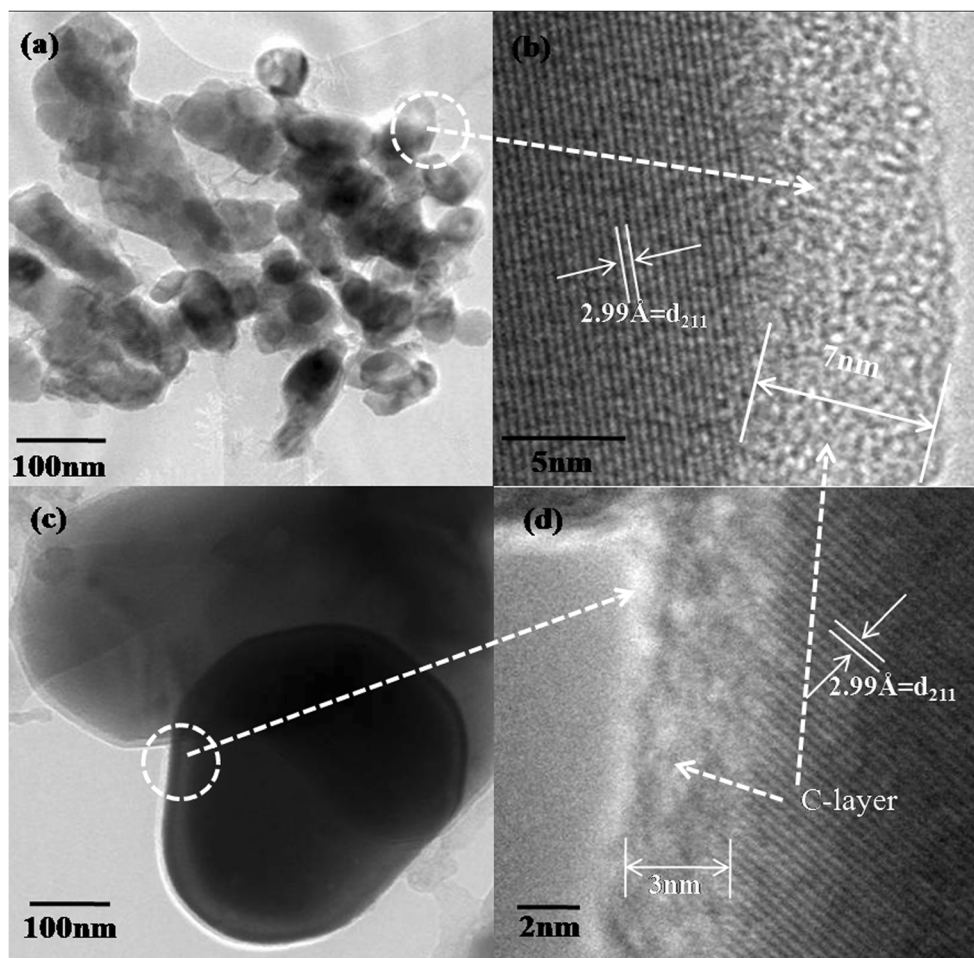Fig. 7 Raman spectra of the samples LFP(0.5) and LFP(1.0) showing the D- and G-bands

Fig. 8 LFP(1.0): **a** particle morphology and **b** lattice image of the LFP overlapped with partially graphitized carbon; LFP(0.5): **c** particle morphology and **d** lattice image of LFP overlapped with partially graphitized carbon

$$i_0 = \frac{RTA}{nFR_{ct}} \qquad (5)$$

where R is gas constant (8.314 Jmol^{-1} K^{-1}), A is surface area of the electrode, F is faraday constant (96,487 Cmol^{-1}), T is working temperature (300 K), and n is number of Li$^+$ transferred per LiFePO$_4$ molecule (=1). The sample LFP(1.0) reflects good electrochemical reversibility by showing better exchange current density(i_0) of 6.94×10^{-5} mAcm^{-2} as compared to 5.17×10^{-5} mAcm^{-2} for LFP(0.5).
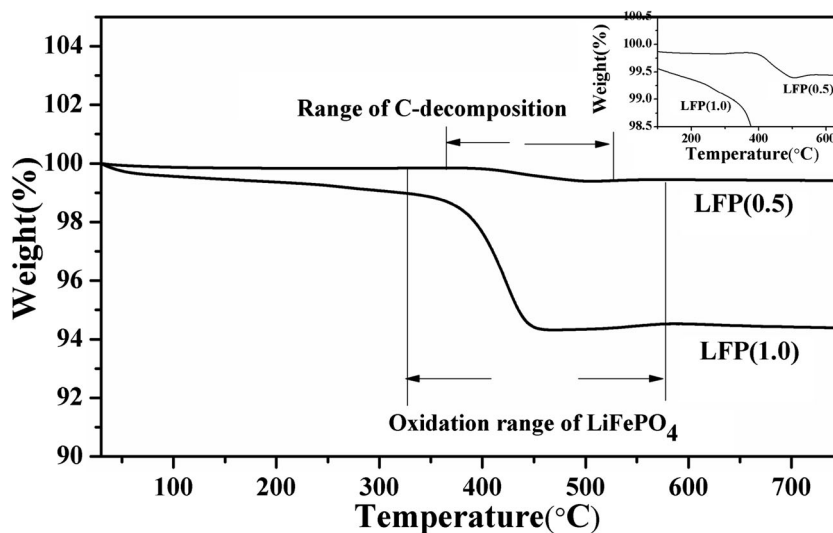
Fig. 9 TG traces of LFP(1.0) and LFP(0.5)

Table 1 Showing weight of carbon in LFP/C by addition of aniline monomer

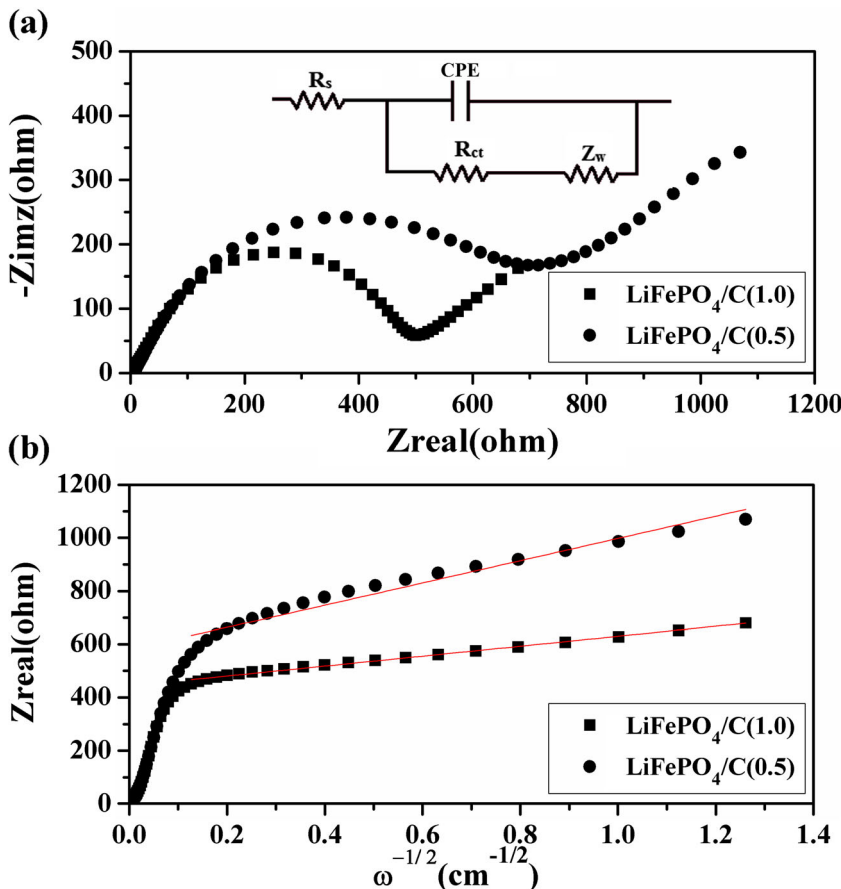| Aniline (volume, ml)	Aniline (weight, g)	Polyaniline (weight, g)	Polymerization (yield, %)	Weight of LFP (g)	Wt% of carbon in LFP/C	Weight of carbon (g)
1.0	1.02	0.8671	85	3.84	9.67	0.3686
0.5	0.51	0.4386	86	3.81	5.52	0.2076

The diffusion coefficient of Li^+ can be calculated using the following equation [29]:

$$D_{Li^+} = \frac{R^2 T^2}{2A^2 n^4 F c^2 \sigma^2}$$ (6)

where C is the concentration of Li^+ ($\sim 1.57 \times 10^{-2}$ mol cm^{-3}) and σ is Warburg factor. The value of σ can be calculated from the slope of linearly fitted Z_{real} vs $\omega^{-1/2}$ line (Fig. 10b) in the low angular frequency region. The diffusion coefficient as calculated from Equation (3) for the samples LFP(1.0) and LFP(0.5) were 6.82×10^{-15} and 1.35×10^{-15} cm^2 s^{-1}, respectively. The higher diffusion coefficient for sample LFP(1.0) reflects the better kinetic to Li^+ during charging/discharging of electrode.
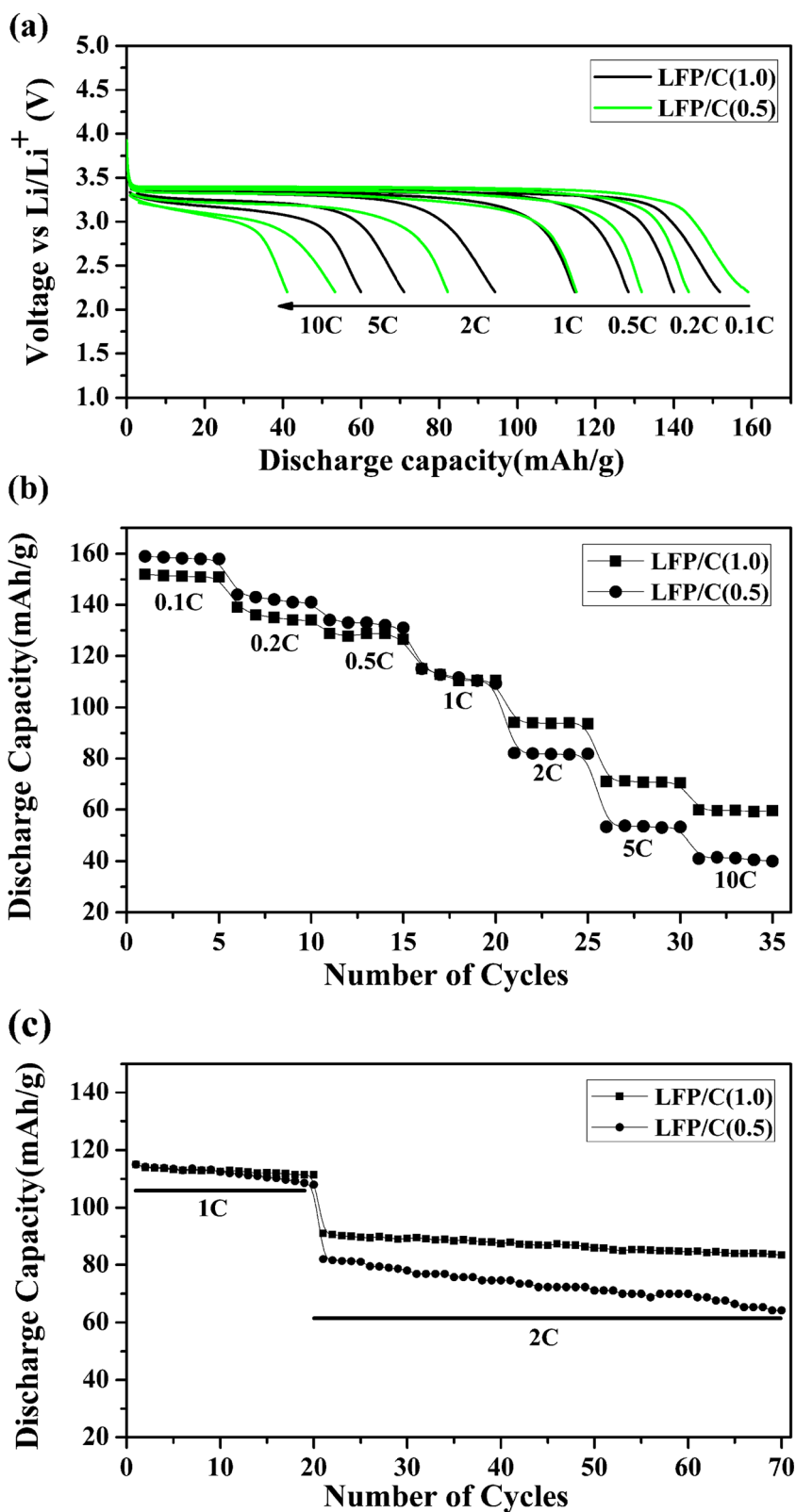
Electrochemical performance

The galvanostatic charging/discharging of LFP(1.0) and LFP(0.5) samples were determined between 2.2 and 4 V at various current rates of 0.1, 0.2, 0.5, 1, 2, 5, and 10 C. The discharge profiles of samples are shown in Fig. 11a. The highest discharge capacities of 159 and 152 mAh g^{-1} were gained at 0.1 C rate for the samples LFP(0.5) and LFP(1.0), respectively. At 0.1 and 0.2 C rate, the sample LFP(0.5) shows a higher capacity as compared to LFP(1.0). As the rate of charging/discharging further increase to 1 C, both the materials show nearly the same discharge capacity. Sample LFP(1.0) shows higher discharge capacity of 94 mAh g^{-1} as compared to 82 mAh g^{-1} for LFP(0.5) at 2 C rate. The sample LFP(1.0) shows higher rate capability of 60 mAh g^{-1} at 10 C rate. Figure 11b shows the cyclability of the samples at various current rates (0.1, 0.2, 0.5, 1, 2, 5, and 10 C) for 35 cycles. The


Fig. 10 **a** Electrochemical impedance spectra of LFP(1.0) and LFP(0.5), and **b** linear fitting of Warburg impedance of sample LFP(1.0) and LFP(0.5)

poor rate capability of sample LFP(0.5) is attributed by the low electronic and ionic conductivity as confirmed by electrochemical impedance spectroscopy. Figure 11c shows the

cyclic stability of the samples at 1 C (20 cycles) and 2 C (50 cycles) rates for 70 cycles. The sample LFP(1.0) shows good cyclic stability as compared to LFP(0.5).

Fig. 12 a Cyclic voltammogram of LFP(0.5) and **b** LFP(1.0) at a scanning rate 0.1 mV s^{-1}, shows oxidation/reduction peaks for 3 cycles
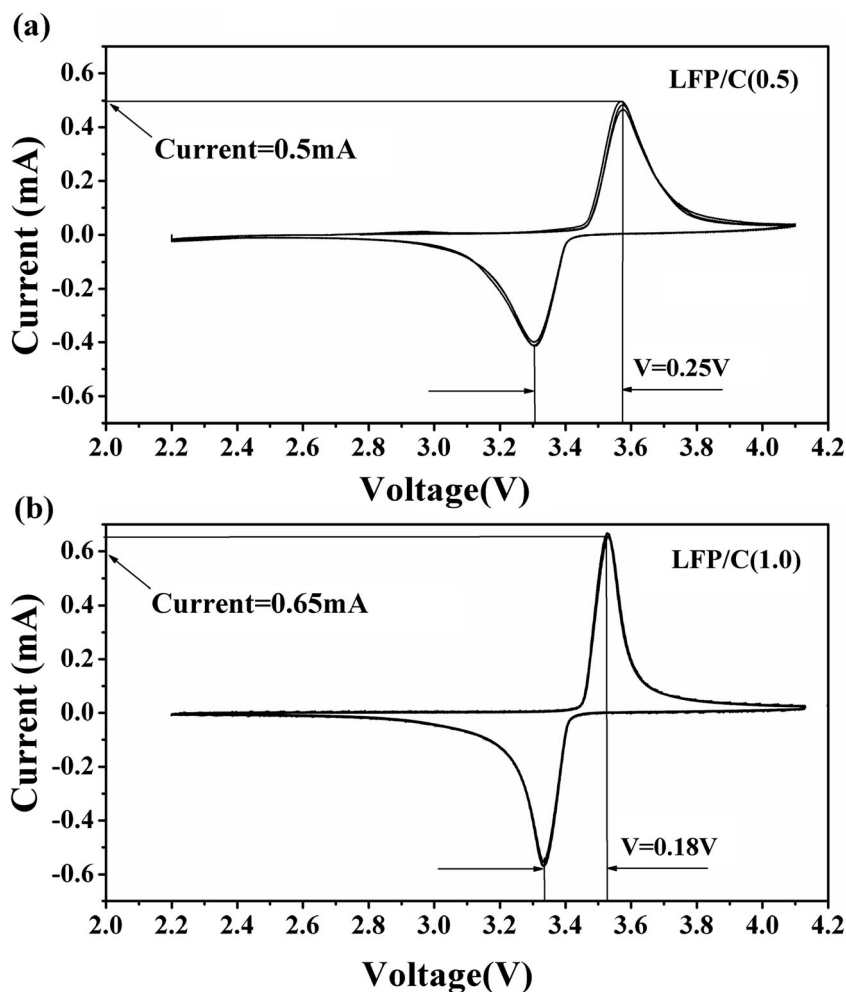
At slow rate (0.1 C), the Li$^+$ diffusion is slow enough that the particle size and carbon coating do not have a significant effect on conduction so that the discharge capacity of both materials are nearly comparable. Though at 0.1 C rate, the composite LFP(0.5) shows better discharge capacity due to lower fraction of inactive carbon present in the composite material [11]. For the charging/discharging rate of 0.2 C discharge capacity of sample LFP(1.0) was reduced due to the presence of less LFP oxide material. The carbon network formed on the LFP particle was electrochemically inactive to storage Li$^+$. So, overall effect of higher carbon weight at a slow current rate was to decrease the specific capacity of sample LFP(1.0). At a faster rate of charging and discharging, carbon coating thickness, particle size, quality, and uniformity of coating play a major role [30, 31]. Raman spectroscopy confirms the same quality (level of graphitization) of carbon present in both the materials. But the thin carbon coating and larger particle of the sample LFP(0.5) affect adversely the material capacity when charging/discharging occurs at a faster rate. Thin carbon coating may not be sufficient to give better coverage to LiFePO$_4$ which results to less conductivity. Electrochemical impedance analysis reveals that the sample

LFP(1.0) shows better kinetics to Li$^+$ and better electronic conductivity. The larger particle size of LFP(0.5) enhances the diffusion length resulting to increase in the diffusion time for Li$^+$ due to which the material is not able to charge/discharge to its full capacity. So, the net effect is the decrease in discharge capacity of material LFP(0.5) at faster 2, 5, and 10 C rates. The better reversibility as reflected by exchange current density for sample LFP(1.0) electrode reflect the good cyclability of the material.

Cyclic voltammetry test

Figure 12a and b shows the cyclic voltammogram of samples LFP(1.0) and LFP(0.5) for 2 cycles at a constant voltage rate of 0.1 mV s^{-1}, respectively, showing the single reduction and oxidation peak between 2.2 and 4.1 V. The good overlapping of graph for cycles indicates a very low or little capacity fade of material per cycle. The peaks in the cyclic voltammogram reveal fast conduction of Li$^+$ at 3.56 and 3.31 V for sample LFP(0.5), and 3.53 and 3.33 V for sample LFP(1.0), respectively. From the cyclic voltammogram curves, it was found that the potential difference between the oxidation/reduction

peaks is 0.25 and 0.18 V for samples LFP/C(0.5) and LFP/C(1.0), respectively. The narrow potential difference between oxidation/reduction peaks for sample LFP/C(1.0) reflects the small polarization of electrode resulting higher reversibility [32].

Conclusions

Polyaniline gel-coated $(NH_4)Fe(HPO_4)_2$ was synthesized by polymerization of aniline monomers. The growth of $(NH_4)Fe(HPO_4)_2$ particle was restricted due to the polymerization. The decomposition of the polymer coating has resulted in uniform coverage of carbon coating on the LFP particles surface with coating thickness of ~3 and ~7 nm for LFP(0.5) and LFP(1.0), respectively. Raman spectroscopy has revealed that the carbon coating has a good graphitized form. The weight percent of carbon as estimated from the TG analysis is in accordance with the initial amount of aniline monomer used for preparation of both the samples. Discharge capacities of the samples measured up to 105 cycles shown in Fig. 11b (for 35 cycles) and 11c (for 70 cycles) for LFP(1.0) and for LFP(0.5) at 0.1, 0.2, 1, 2, 5, 10, and 20 C rates. The discharge capacities of synthesized materials are found to vary with carbon coating thickness and particle size of LFP. At a slow C rate, the sample LFP(0.5) shows higher discharge capacity as compared to LFP(1.0), but at the faster C rate, LFP(1.0) shows better cyclic stability and discharge capacity as compared to LFP(0.5). The higher capacity and cyclability of LFP(1.0) is attributed by the (1) fine particle size, (2) higher Li^+ diffusion coefficient, and (3) electronic conductivity as confirmed by microscopy and electrochemical impedance spectroscopy analysis. Cyclic voltammetry tests reveal the narrow voltage difference between peak currents in a cycle confirms sample LFP(1.0) shows better reversibility at 0.1 mV s^{-1} scan rate.

References

1. Padhi AK, Nanjundaswamy K, Goodenoug JB (1997) Phospho-olivines as positive-electrode materials for rechargeable lithium batteries. J Electrochem Soc 144:1188–1194
2. Andersson AS, Kalska B, Haggstrom L, Thomas JO (2000) Lithium extraction/insertion in LiFePO4: an X-ray diffraction and Mössbauer spectroscopy study. Solid State Ionics 130:41–52. doi:10.1016/S0167-2738(00)00311-8
3. Yang Z, Xia J, Zhi L, Zhang W, Pei B (2014) An improved solid-state reaction route to Mg^{2+}-doped LiFePO$_4$/C cathode material for Li-ion battery. Ionics 20:169–174. doi:10.1007/s11581-013-0974-2
4. Wang J, Sun X (2012) Understanding and recent development of carbon coating on LiFePO$_4$ cathode materials for lithium-ion batteries. Energy Environ Sci 5:5163–5185. doi:10.1039/C1EE01263K
5. Yamada A, Chung SC, Hinokuma K (2001) Optimized LiFePO$_4$ for lithium battery cathodes. J Electrochem Soc 148(3):A224–A229. doi:10.1149/1.1348257
6. Wu XL, Jiang LY, Cao FF, Guo YG, Wan LJ (2009) LiFePO$_4$ nanoparticles embedded in a nanoporous carbon matrix: superior cathode material for electrochemical energy-storage devices. Adv Mater 21:2710–2714. doi:10.1002/adma.200802998
7. Guo YG, Hu JS, Wan LJ (2008) Nanostructured materials for electrochemical energy conversion and storage devices. Adv Mater 20:2878–2887. doi:10.1002/adma.200800627
8. Xu B, Qian D, Wang Z, Meng YS (2012) Recent progress in cathode materials research for advanced lithium ion batteries. Mater Sci Eng R 73:51–65. doi:10.1016/j.mser.2012.05.003
9. Lv YJ, Su J, Long YF, Lv XY, Wen YX (2014) Effect of milling time on the performance of bowl-like LiFePO4/C prepared by wet milling-assisted spray drying. Ionics 20:471–478. doi:10.1007/s11581-013-1002-2
10. Chen WM, Qie L, Yuan LX, Xia SA, Hu XL, Zhang WX, Huang YH (2011) Insight into the improvement of rate capability and cyclability in LiFePO4/polyaniline composite cathode. Electrochim Acta 56:2689–2695. doi:10.1016/j.electacta.2010.12.041
11. Chena Z, Dahna JR (2002) Reducing carbon in LiFePO$_4$/C composite electrodes to maximize specific energy, volumetric energy, and tap density. J Electrochem Soc 149(9):A1184–A1189. doi:10.1149/1.1498255
12. Masquelier C, Croguennec L (2013) Polyanionic (phosphates, silicates, sulfates) frameworks as electrode materials for rechargeable Li (or Na) batteries. Chem Rev 113:6552–6591. doi:10.1021/cr3001862
13. Kong LB, Zhang P, Liu MC, Liu H, Luo YC, Kang L (2012) Fabrication of promising LiFePO$_4$/C composite with a core–shell structure by a moderate in situ carbothermal reduction method. Electrochim Acta 70:19–24. doi:10.1016/j.electacta.2012.02.102
14. Wang YG, Wang YR, Hosono EJ, Wang KX, Zhou HS (2008) The design of a LiFePO$_4$/Carbon nanocomposite with a core–shell structure and its synthesis by an in situ polymerization restriction method. Angew Chem Int Ed 47:7461–7465. doi:10.1002/anie.200802539
15. Singla ML, Sehrawat R, Rana N, Singh K (2011) Dielectric behaviour of emeraldine base polymer–ZnO nanocomposite film in the low to medium frequency. J Nanoparticle Res 13:2109–2116. doi:10.1007/s11051-010-9968-4
16. Kang ET, Neoh KG, Tan KL (1998) Polyaniline: a polymer with many interesting intrinsic redox states. Prog Polym Sci 23:277–324. doi:10.1016/S0079-6700(97)00030-0
17. Kulkarni M, Kale B, Apte S, Naik S, Mulik U, Amalnerkar D (2011) Synthesis and characterization of polyaniline nanofibres by rapid liquid-liquid interfacial polymerization method. Chem Chem Technol 5:55–58
18. Zaghib K, Julien CM (2005) Structure and electrochemistry of FePO$_4$.2H$_2$O hydrate. J Power Sources 142:279–284. doi:10.1016/j.jpowsour.2004.09.042
19. Wang YG, Li HQ, Xia YY (2006) Ordered whisker like polyaniline grown on the surface of mesoporous carbon and its electrochemical capacitance performance. Adv Mater 18:2619–2623. doi:10.1002/adma.200600445
20. Scaccic S, Carewska M, Bartolomeo AD, Prosini PP (2002) Thermoanalytical investigation of iron phosphate obtained by spontaneous precipitation from aqueous solutions. Thermochim Acta 383:145–152. doi:10.1016/S0040-6031(01)00686-4
21. Wilcox JD, Doeff MM, Marcinek M, Kostecki R (2007) Factors influencing the quality of carbon coatings on LiFePO$_4$. J Electrochem Soc 154(5):A389–A395. doi:10.1149/1.2667591

22. Kostic R, Miric M, Radic T, Radovic M, Gajic R, Popovic ZV (2009) Optical characterization of graphene and highly oriented pyrolytic graphite. Acta Phys Pol A 116:718–721

23. Reich S, Thomsen C (2004) Raman spectroscopy of graphite. Phil Trans R Soc Lond A 362:2271–2288. doi:10.1098/rsta.2004.1454

24. Dresselhaus MS, Jorio A, Saito R (2010) Characterizing graphene, graphite, and carbon nanotubes by Raman spectroscopy. Annu Rev Condens Matter Phys 1:89–108. doi:10.1146/annurev-conmatphys-070909-103919

25. Vujkovic M, Stojkovic I, Cvjeticanin N, Mentus S (2003) Gel-combustion synthesis of LiFePO$_4$/C composite with improved capacity retention in aerated aqueous electrolyte solution. Electrochim Acta 92:248–256. doi:10.1016/j.electacta.2013.01.030

26. Zhang H, Liu D, Qian X, Zhao C, Xu Y (2014) A novel nano structured LiFePO$_4$/C composite as cathode for Li-ion batteries. J Power Sources 249:431–434. doi:10.1016/j.jpowsour.2013.10.109

27. Zhao SX, Ding H, Wang YC, Li BH, Nan CW (2013) Improving rate performance of LiFePO$_4$ cathode materials by hybrid coating of nano-Li$_3$PO$_4$ and carbon. J Alloys Compd 566:206–211. doi:10.1016/j.jallcom.2013.03.041

28. Gao F, Tang Z (2008) Kinetic behavior of LiFePO$_4$/C cathode material for lithium-ion batteries. Electrochim Acta 53:5071–5075. doi:10.1016/j.electacta.2007.10.069

29. Shu H, Wang X, Wu Q, Liu L, Liang Q, Yang S, Ju B, Yang X, Zhang X, Wang Y, Wei Q, Hu B, Liao Y, Jiang H (2012) The effect of ammonia concentration on the morphology and electrochemical properties of LiFePO$_4$ synthesized by ammonia assisted hydrothermal route. Electrochim Acta 76:120–129. doi:10.1016/j.electacta.2012.04.156

30. Dominko R, Bele M, Gaberscek M, Remskar M, Hanzel D, Pejovnik S, Jamnika J (2005) Impact of the carbon coating thickness on the electrochemical performance of LiFePO$_4$ÕC composites. J Electrochem Soc 152(3):A607–A610. doi:10.1149/1.1860492

31. Cho YD, Fey GTK, Kao HM (2009) The effect of carbon coating thickness on the capacity of LiFePO$_4$/C composite cathodes. J Power Sources 189:256–262. doi:10.1016/j.jpowsour.2008.09.053

32. Zhang W, Hu Y, Tao X, Huang H, Gan Y, Wang C (2010) Synthesis of spherical LiFePO$_4$/C via Ni doping. J Phys Chem Solids 71:1196–1200. doi:10.1016/j.jpcs.2010.04.015